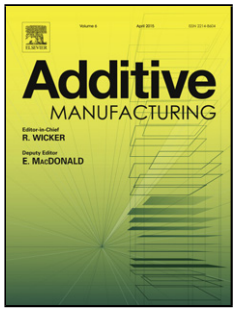

Laser sintering of graphene nanoplatelets encapsulated polyamide powders

Binling Chen (Formal analysis) (Investigation) (Writing - original draft), Richard Davies (Methodology) (Writing - review and editing), Yaan Liu (Formal analysis) (Writing - review and editing), Nan Yi (Formal analysis) (Writing - review and editing), Dayuan Qiang (Writing - review and editing), Yanqiu Zhu<ce:contributor-role>Writing - review and editing), Oana Ghita (Conceptualization) (Supervision) (Writing - review and editing)

PII: S2214-8604(20)30735-1

DOI: https://doi.org/10.1016/j.addma.2020.101363

Reference: ADDMA 101363

To appear in: *Additive Manufacturing*

Received Date: 6 December 2019

Revised Date: 30 March 2020

Accepted Date: 26 May 2020

Please cite this article as: Chen B, Davies R, Liu Y, Yi N, Qiang D, Zhu Y, Ghita O, Laser sintering of graphene nanoplatelets encapsulated polyamide powders, *Additive Manufacturing* (2020), doi: https://doi.org/10.1016/j.addma.2020.101363

Laser sintering of graphene nanoplatelets encapsulated polyamide powders

Binling Chen[a]*, Richard Davies[a], Yaan Liu[a], Nan Yi[a], Dayuan Qiang[a], Yanqiu Zhu[a], Oana Ghita[a]

[a]College of Engineering, Mathematics and Physical Sciences, University of Exeter, Exeter, EX4 4QF, UK

* E-mail: B.Chen@exeter.ac.uk

Graphical abstract

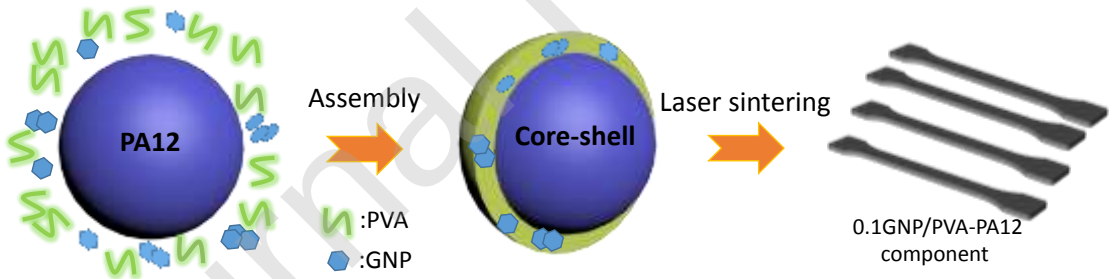

Abstract

This paper presents a comprehensive study in the fabrication and safety of new nanocomposite powders for laser sintering. The nanocomposite powder is based on a

core-shell structure where nanoparticles (graphene nanoplatelets, GNP) are encapsulated on the surface of the polymeric particles (polyamides PA12) in a thin layer of poly(vinyl alcohol) (PVA). Powder rheology data as well as SEM and TEM showed that GNP was dispersed well in the PVA coating and improved flow. Half time crystallisation kinetics was used to determine differences induced in the polymer and the laser sintering process by the presence of GNP. Nanosafety aspects, critical in a manufacturing environment, are also considered here and exposure monitoring tests were carried out. Results confirmed a low nanoparticle air exposure and therefore confirmed the successful surface encapsulation of the GNP in nanocomposite powders. The laser sintered 0.1GNP/PVA-PA12 parts showed enhanced mechanical properties in tensile, compression and 3-point bending test.

Keywords: Nanocomposites Powders; Powder Bed Fusion; Laser Sintering; Nanosafety; Coreshell Structure

1. Introduction

Additive manufacturing (AM) is an advanced processing technology building components layer-by-layer. Of the various AM technologies, laser sintering (LS) is considered one of the most economically viable and robust technologies for small scale series manufacturing.

Although the choice of plain polymeric powders for laser sintering has been increasing over the last five years, the demand for functional components requires further developments in methods of incorporation of fillers, and fibrous additives.

PA 3200 GF (glass bead filled polyamide 12 powder) and CarbonMide® (carbon-fibre reinforced polyamide 12 powder) [1] are two commonly used laser sintering commercial blend composite grades. Traditionally, dry-mixing and melt-mixing were the two main methods for the preparation of composites [2, 3]. However, considering the health and safety aspects, the quality of nanoparticle dispersion, and extensive energy consumption issues of the melt compounding and milling, novel preparation methods had been proposed by various research groups. Studies on the PA incorporation of various fillers such as silica [4], modified montmorillonite [5], short carbon fibre [6, 7] have been developed by Yan's group.

Mo et al. developed a method to produce polyamide (PA12) based nanocomposite powders for LS [8-11]. Nanoparticles were attached to the surface of the PA12 particles by softening the surface of the PA12 particles with the aid of a selective liquid at high temperatures and pressures. The results showed carbon nanotubes (CNT) were homogenously distributed on the surface of the PA12 particles [8]. However, the interactions between CNT and PA12 particles, depth of penetration of CNTs onto the surface were not investigated although critical for health and safety especially when operating with large quantities of nanocomposite powders in a dry environment.

Another method proposed is based on the chemical reduction of graphene oxide (GO) onto the surface of PA12 particles. Pentzer et al. [12] reported that PA12 powders were first dispersed into a GO aqueous solution. The GO nanosheets were deposited onto the PA12 particles due to the increased solution ionic strength. This method requires extra chemicals such as sodium chloride and hydrazine, and it is suitable for GO applications only. Moreover, no data of interaction between GO and

PA12 particles is provided. A working electrostatic motor was then fabricated via laser sintering using these composite powders.

More recently, Gökce et al. reported a preparation approach where surfactant-free laser-generated colloidal nanoparticles were adsorbed onto the surface of PA12 particles directly in an aqueous solution [13]. This approach is only suitable for metal and oxide nanoparticles, and the interaction between nanoparticles and PA12 such as surface charge needs to be further analysed. No components have been laser sintered yet.

A previous study of the authors provided a new method to fabricate polymeric nanocomposite powders using a core-shell structure strategy, where polyetherimide (PEI) was used as a shell on the surface of a core, poly ether ether ketone (PEEK) particle [14]. Nanoparticles such as GNP and inorganic fullerene-like tungsten disulfide (IF-WS_2) in concentrations of 0.1, 1, and 5 wt% were incorporated in the PEI shell structure. However, the GNP and IF-SW_2 PEI/PEEK powder were not tested in the laser sintering process. The current study not only proposes a new combination of polymers for the core-shell structures showing the potential offered by the fabrication method of the nanocomposite powders, but laser sinters the powders in a commercial powder bed AM system and provides a comprehensive set of mechanical results of the new nanocomposite parts. GNP were encapsulated in a Polyvinyl alcohol (PVA) shell on PA12 core particles. The PVA is a polymer soluble in water with thermal characteristics similar to that of PA12 (e.g. melting point is close to that of PA12). The powder flow tests showed an improved flowability of PVA coated PA12 powders when compared with the plain PA12 powder. It was found the addition of GNP changed the thermal

behaviour of the nanocomposite powders and further affected the LS processing parameters (e.g. powder bed temperature). The nanosafety aspects were also considered, being the first study to monitor the nanoparticle exposure in air during LS. The nanoparticle exposure levels of GNP-PA12 dry-mix powder, and the encapsulated GNP through a core-shell structure, were monitored and compared, thus confirming the successful encapsulation of the GNP into the core-shell powders. The laser-sintered parts of PVA-PA12 and 0.1GNP/PVA-PA12 have been successfully fabricated using an EOS P 100 system. The enhanced mechanical properties of the core-shell sintered parts confirm the benefits of good dispersion of nanoparticles.

2. Materials and methods

2.1 Materials

The commercial grade EOS PA2200 (Polyamide 12, PA12, or Nylon12) powder (M_w=29,000 g/mol) was used as the core particles; PVA (Polyvinyl alcohol) (M_w=89,000-98,000 g/mol) purchased from Sigma-Aldrich was used as a coating; GNP (Graphene nanoplatelets) were purchased from Thomas Swan & Co Ltd.

2.2 *Preparation of PVA coated PA12 powder (referred to as PVA-PA12)*

PVA granules were dissolved in distilled water. PA12 powder was then added to the water. A solution of PVA, distilled water and PA12 was prepared in a weight ratio of 1:250:50 (PVA: H_2O: PA12). Following a strong ultrasonic treatment (Qsonica sonicator Model Q125, 75 Watts and 20 kHz) for 20 minutes and careful removal of water by heating, the collected powder was dried in an oven at 85° C for 48 hours. The dried

powder was gently ground to break down any agglomeration which was formed during drying.

2.3 Preparation of the core-shell particles with nanoparticles (referred to as 0.1GNP/PVA-PA12, 1GNP/PVA-PA12)

The process was similar to the preparation of the PVA coated PA12. Nanoparticles were added after the PVA was fully dissolved prior to adding PA12 particles. GNP was added at 0.1 or 1 wt % of the total amount of PVA and PA12.

*2.4 Fabrication of laser-sintered part*s

The laser sintering system used in this study is an EOS P100 Formiga. The processing details of powders are listed below in Table 1.

Table 1 The LS processing parameters for PA12, PVA-PA12 and 0.1GNP-PVA-PA12

Material	Bed temperature, T_b (°C)	Laser power, (W)	Laser speed, (mm/s)	Hatching distance, mm	Energy density, (J/mm^2)
PA12	169	21	2500	0.25	0.0336
PVA-PA12	173	21	2500	0.25	0.0336
0.1GNP-PVA-PA12	172	21	2500	0.25	0.0336

2.5 Morphology test

SEM images were obtained by a Nova Nanolab 600 scanning electron microscope at an acceleration voltage of 20 kV. Powders and the laser-sintered tensile bars were first spread or pasted on a conductive carbon tape. A thin layer of gold coating was then sputtered onto the samples. The TEM images were recorded by using a JOEL-2100 TEM at a voltage of 200 kV. The powders were first dispersed in isopropyl alcohol under sonication for 20 minutes, and then pipetted onto a holey carbon Cu grid to

form TEM specimens. In order to investigate the cross-section of the powders, samples were first mixed with a thermoset resin (TAAB Laboratories, Aldermaston, UK). This mixture was placed in a plastic capsule and polymerized at 60 °C for 24 hours. A70 nm ultrathin sections were obtained by using an RMC POWERTOME PC Ultracut, and they were then collected on pioloform-coated EM 100 mesh copper TEM grids.

2.6 Thermal Characterisation

A Mettler Toledo DSC 821e/700 was used to measure melting, crystallisation and glass transition temperatures. Nitrogen with a flow rate of 50 ml min^{-1} was used as it is an inert gas. The samples were heated in DSC from 25 °C to 250 °C at a heating rate of 10 °C min^{-1}, and then cool from 250 °C to 25 °C with a heating rate of 10 °C min^{-1}. Three repeats of each sample were carried out. For isothermal tests, the sample was heated to 250 °C, and then rapidly cooled (at a cooling rate of 80 °C min^{-1}) to the desired isothermal temperature of 152 °C, 157 °C, 160 °C, 162 °C and 167 °C, respectively. The melt flow index (MFI) of the powders were measured by using Melt Flow Tester 6941 CEAST at 185 °C based on the ISO standard 1133 with a material heating time of 10 min. The materials were extruded through a tubular die (D = 2 mm and L = 80 mm). Five repeats of tests were carried out for each material.

2.7 Particle test

The size and shape of powders were measured using a Microtrac Sync analyser, which combines laser diffraction technology with dynamic image analysis to measure the particle size and shape in a single step. The particle size was determined by the intensity of scattered light and the particle shape was recorded by a high-speed digital camera. Around 4000-6000 particles were captured and analysed in each measurement. Three measurements were repeated for each material. A Freeman FT-

4 powder rheometer was used to assess powder flow properties at room temperature. Dynamic properties such as Basic Flow Energy (BFE), Specific Energy (SE) and Stability Index (SI) were obtained from the combined stability and variable flow rate test. BFE was measured during the downward blade movement. It provides information on flowability, regarding the difficulty on displacing the powder. The SE was measured by lifting the powder from the bottom of the vessel to the top in an unconfined state.

2.8 Nanoparticles exposure in air test

A Naneos Partector 2 Aerosol Dosimeter (Naneos Particle Solutions GmbH) was used to monitor the presence of GNP in air when handling the powders. The system has a wide concentration measurement range from 0 to 12000 μm^2 cm^{-3} and a wide particle size measurement range from 10 nm to 300 nm. The Partector measures the lung deposited surface area (LDSA) in m^2 cm^{-3}, which is considered the most relevant metric for the health effects of high aspect ratio nanoparticles on humans. 50 g of each powder, plain PA 12, 1GNP-PA12 dry-mixed, 0.1GNP/PVA-PA12 and 1GNP/PVA-PA12, was transferred from beaker to beaker by pouring action in an extraction cabinet for 3 mins, respectively. LDSA was monitored by positioning the Naneos Paratector at different locations within the fume cupboard (at a high level well above the area where the powder transfer takes place and at a low level at a similar height as the powder transfer). Four repeat measurements were carried in each location. The air monitor recorded data in three steps: 10-minute Stabilisation; 3-minute mixing; and 10-minute Stabilisation.

2.9 Mechanical Characterisation

ISO 527-2-1BA tensile specimens were laser sintered. The specimen length is 75 mm, gauge length is 25 mm, and gauge width is 5 mm. Tensile testing experiments were performed by using a Universal Shimadzu AGS-X Series Tensile Tester at room temperature. The testing speed was 1 mm min^{-1}. Compression samples were manufactured with ISO 604 geometries, where the diameter is 10 mm and thickness is 4 mm. Compression tests were carried out using Lloyd LR300k Universal Materials Testing Machine. The testing speed was 5 mm min^{-1}. 3-point bending test samples were made with ISO 178 geometries, where the length is 80 mm, width is 10 mm, and thickness is 4 mm. The span size was 64 mm and the speed was 1 mm min^{-1}. 10 repeat measurements of each material for each mechanical test were carried out. The dimensions of laser sintered specimens are slightly different from the CAD model however, the actual size values of each specimen were applied for each mechanical test.

2.10 Statistical analyses

Statistical analyses were performed using JMP (SAS, Version 15.0.0), including one-way ANOVA for single factor analyse and Tukey-Kramer HSD for means comparisons. Significant differences were assessed in terms of 'p-values' with a threshold of 0.05. Any p-value found smaller than 0.05 means that there is a significant difference between the compared groups of data. Significant difference indicates that the variation of the means values between two or more datasets is not due to the natural variation of the results, but to the conditions with whom the data were generated.

3. Results and discussion

3.1 Characterisation of PA12, PVA-PA12, 0.1GNP/PVA-PA12 and 1GNP/PVA-PA12 Powders

SEM images (Fig. 1) were taken to investigate the changes in surface morphology of the newly coated particles and to identify the presence of GNP. Fig. 1a and Fig. 1b show the SEM images of plain PA12 powders. The particle surface of PA12 powder is not very smooth due to the nature of the synthesis process. In the case of the core-shell PVA-PA12 powders (Fig. 1c-1f), the surface appears smoother. The PVA-PA12 and 1GNP/PVA-PA12 powders have a similar particle size as the plain PA12 (shown in Fig. 1c and Fig. 1e), suggesting the PVA coating layer is very thin. This is also confirmed by the TEM images of particles cross-section area shown in Fig. 2. The thickness of PVA layer is approximately 1 μm. In addition, Fig. 1f shows that the GNP were well embedded into the PVA coating layer, also confirmed by Fig. S1. The particle morphology of 0.1GNP/PVA-PA12 is similar to that of 1GNP/PVA-PA12 (Fig. S2).

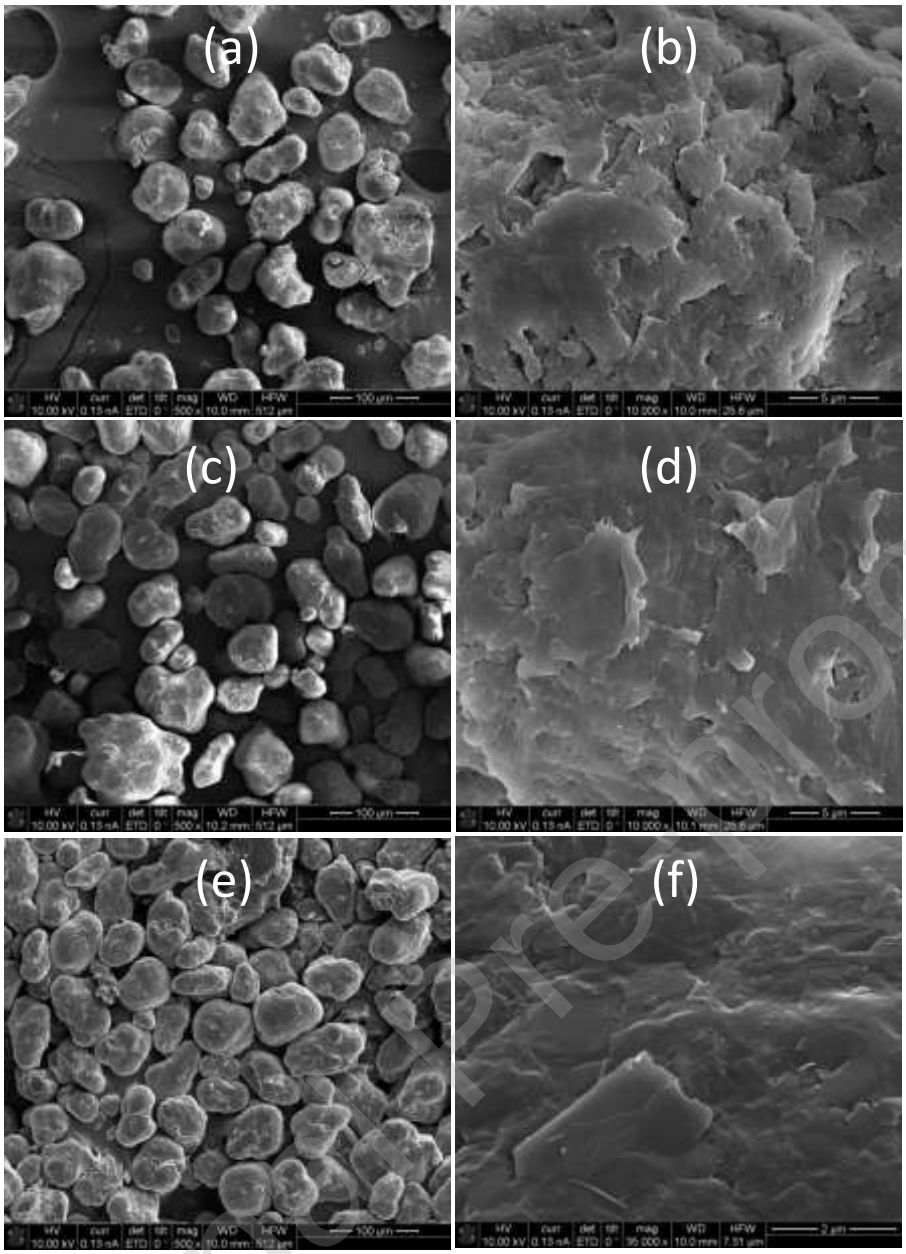

Fig. 1. SEM images of (a), (b) typical PA12 powder at different magnification; (c), (d) PVA-PA12 powder, the surface of the particles seems to be slightly smoother; and (e), (f) 1GNP/PVA-PA12 powder, GNP were well embedded into the PVA coating layer.

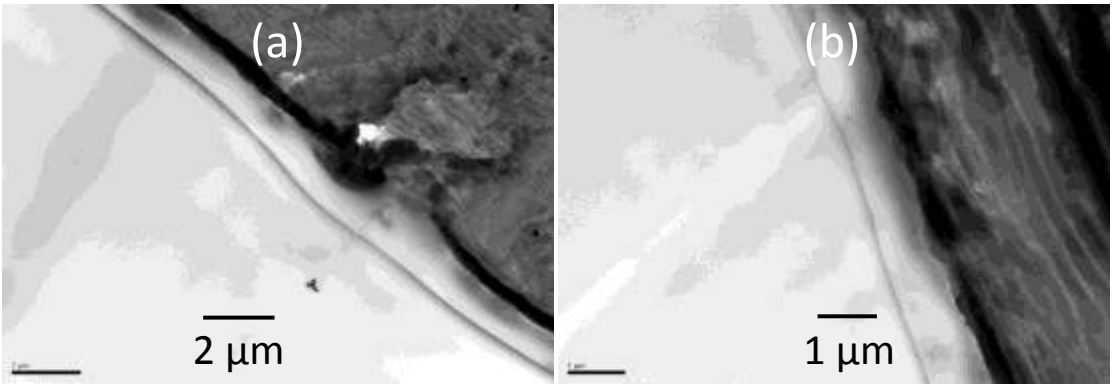

Fig. 2. TEM images of the cross-section area of PVA-PA12 particle, the darker region represents the main bulk PA12 particle, and the thin light grey layer represents the PVA shell.

The particle size distribution (PSD) of the plain PA12 and PVA coated PA12 powders can be seen in Fig. 3. There is little difference between the grades of powders indicating that the fabrication process of the nanocomposite powders did not affect the PSD. In addition, both sphericity and circularity data of the plain PA12 and coated powders (Fig. S3 and Fig. S4) show similar results, indicating the PVA coating did not affect the particle shapes either.

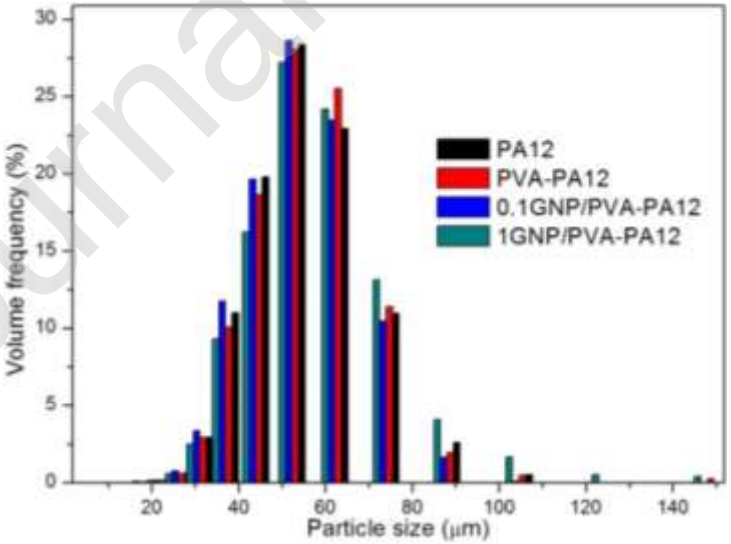

Fig. 3. Particle size distribution of PA12, PVA-PA12, 0.1GNP/PVA-PA12 and 1GNP/PVA-PA12 powders

3.2 Thermal analysis and crystallisation kinetic studies

The onset melting and onset crystallisation temperatures of the nanocomposite powders were analysed by DSC (shown in Fig.4 and Fig. S5) and compared with the plain and the core-shell particles without GNP. Fig. 4 shows the DSC curves of all powders and the thermal properties are listed in Table 2. The purpose of using DSC is to understand the effect PVA and GNP on the crystallisation of PA12 and subsequently help to define temperatures for LS [15]. The onset of crystallisation changes amongst the four powders PVA-PA12, 0.1GNP/PVA-PA12 and 1GNP/PVA-PA12 displaying a narrower super-cooling window in comparison with the plain PA12 powder. Koulouri et al. [16] studied the miscibility and crystallisation behaviour of PVA/PA 6 blends and found good miscibility between the two polymers and an improved crystallinity for the compositions rich in PA 6. Similarly, our PVA-PA12 powder exhibits a shifted crystallisation temperature due to a good miscibility and it is possible that PVA facilitates the crystallisation. The crystallisation temperature of the 0.1GNP/PVA-PA12 and 1GNP/PVA-PA12 nanocomposite powders was 0.5 °C and 2.6 °C higher than PVA-PA12, respectively, which suggests that the GNP acted as a nucleating agent and had a nucleation effect on the PVA-PA12.

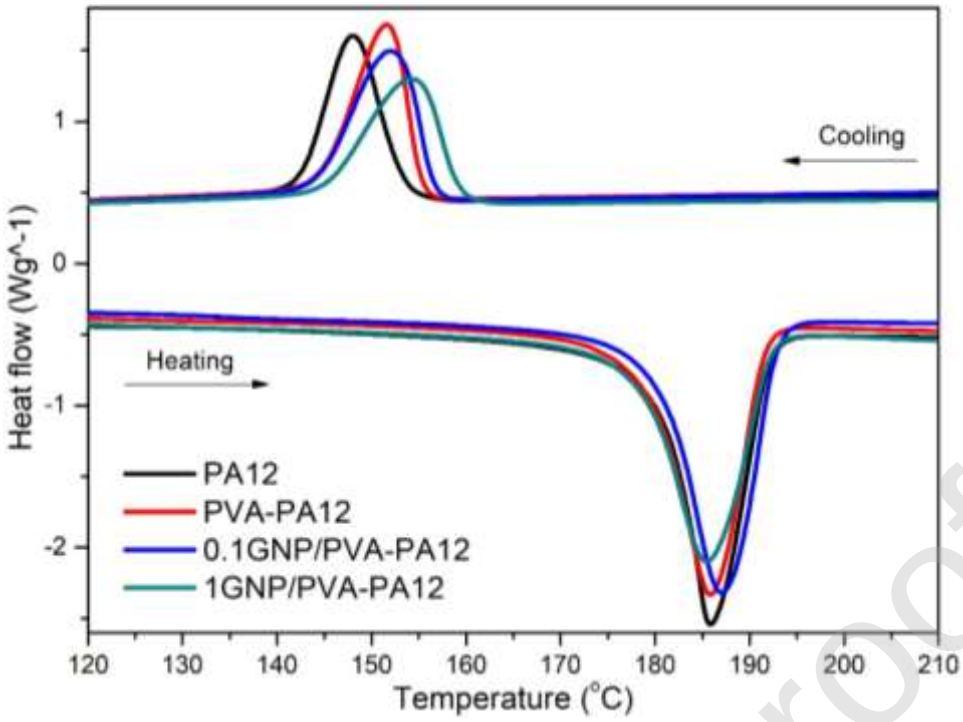

Fig. 4. DSC curves of endothermic and exothermic phase changes during a heating and cooling cycle at 10 °C min^{-1} for plain PA12 and PVA coated PA12 with and without GNP.

Table 2. DSC results for PA and PVA coated powders

Material	Onset melting temperature (°C)	Onset crystallisation temperature (°C)	Crystallisation temperature (°C)	Crystallinity (X_c, %)
PA12	180.8 ± 0.1	153.1 ± 0.4	147.5 ± 0.5	23.6 ± 0.4
PVA-PA12	178.9 ± 0.1	155.2 ± 0.2	151.6 ± 0.1	24.4 ± 0.1
0.1GNP/PVA-PA12	180.1 ± 0.1	156.8 ± 0.1	152.1 ± 0.2	26.2 ± 0.6
1GNP/PVA-PA12	177.9 ± 0.5	159.3 ± 0.2	154.2 ± 0.1	24.6 ± 0.2

The influences of PVA coating and the presence of GNP on the crystallisation kinetics were studied further through isothermal tests. The DSC isothermal traces at 162 °C are shown in Fig. 5a. Based on these isothermal traces, the half time

crystallisation times as a function of crystallisation temperatures were plotted in Fig. 5b. The DSC traces and ½ time crystallisation trends for 152 °C, 157 °C, 160 °C and 167 °C are shown in Fig. S6. Table 3 includes the ½ time crystallisation values of all powders. It can be observed that as the isothermal temperature increases, the peak time of crystallisation is considerably longer. The PVA-PA12 powders had a lower half-time crystallisation than plain PA12. The GNP encapsulated PVA-PA12 powders had an even lower crystallisation half-time than PVA-PA12 powders. This confirms that the PVA and GNP accelerate the crystallisation. Faster crystallisation rates impact on the retraction and shrinkage rates of the molten films, raising the risk of part failure due to curling and warping of the layers. Based on the crystallisation kinetic results, the bed temperature applied for laser sintering GNP-PVA/PA12 powders was increased by approximately 4 °C.

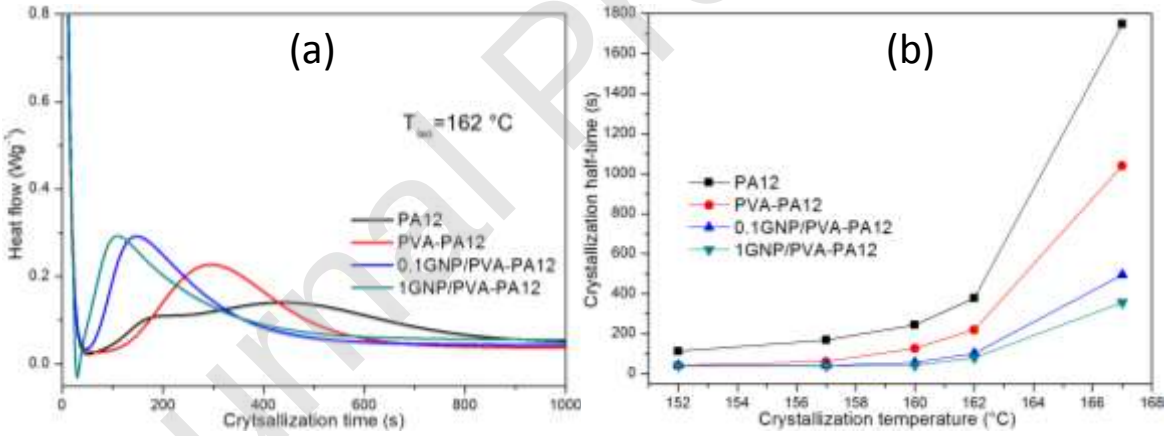

Fig. 5. (a) DSC isothermal traces at 162 °C and (b) Half time crystallisation as function of crystallisation temperature of plain PA12, PVA-PA12, and GNP/PVA-PA12 nanocomposite powders

Table 3. Half time crystallisation values of all powders

	Half time crystallisation at different temperatures (s)				
	152 °C	**157 °C**	**160 °C**	**162 °C**	**167 °C**
PA12	112	169	244	377	1749
PVA-PA12	43	61	127	220	1040
0.1GNP/PVA-PA12	41	42	57	102	494
1GNP/PVA-PA12	39	40	42	81	357

In order to study the influence of PVA coating and the presence of GNP on the rheological behaviour of powders during LS, the Melt Flow Index (MFI) measurements were carried out and are listed in Table 4. Compared to plain PA12 (11.79 g/10min), the flow rate of PVA-PA12 is much lower (2.63 g/10min), which means the addition of PVA makes the new polymeric blend more viscous, which would impact the particle to particle flow and melt film forming during LS. This was due to the fact that the PVA selected had a higher molecular weight of (M_w=89,000-98,000) than that of plain PA12 (M_w=29000). The presence of GNP further affected the melt flow rate in comparison with PVA-PA12. GNP at low concentration (0.1 wt%) seems to have no influence on the flow. 1GNP/PVA-PA12 shows an increased flow rate of 3.19 g/10min. Altay et al. [17] reported that GNP in polypropylene at 1.5 or 3 wt% concentration acts as a lubricant and improves the melt flow. GNP is an atomically smooth 2D material with low surface energy. It is able to reduce adhesion and thus improve the melt flow [18]. GNP in our 1GNP/PVA-PA12 seems to play the same role as Altay's [17].

Table 4. MFI of plain, core-shell and nanocomposite powders at 185 °C

Powder	PA12	PVA-PA12	0.1GNP/PVA-PA12	1GNP/PVA-PA12
Flow rate (g/10 min)	11.79 ± 0.52	2.63 ± 0.12	2.22 ± 0.31	3.19 ± 0.18

3.3 Powder rheology analysis

The powder rheology properties of powders have been measured using a Freeman FT4 rheometer. The results are listed in Table 5. The BFE value for plain PA12 is the highest found for the materials studied here, requiring approximately 208.18 mJ of energy to displace the powder in a confined environment at each rotation. The addition of the PVA shell lowered the BFE value from 208.18 mJ for PA12 to 155.26 mJ for PVA-PA12. This means that the PVA coated powder needs less energy to be displaced at each rotation, suggesting that the PVA coating changes the surface of the particles, creating a smooth surface. Furthermore, the incorporation of GNP further lowered the BFE value from 155.26 mJ for PVA-PA12 to 113.70 mJ for 1GNP/PVA-PA12, suggesting that the GNP has a similar effect as the PVA coating of reducing the surface roughness and allowing a better flow, reducing friction and improving the sliding effect amongst particles.

The SE values of the measured powders have a similar trend to those of the BFE values. Plain PA12 powder requires more energy to be lifted up by the blade, having a value of 6.61 mJ/g. PVA-PA12, 0.1GNP/PVA-PA12 and 1GNP/PVA-PA12 have a SE value of 6.17, 5.20, and 5.33, respectively, suggesting that less energy is required to lift the PVA coated PA12 particles when in a low stress environment than plain PA12.

All of the powders show similar values of Conditioned Bulk Density (CBD), an indication that the packing density remained the same and that the particle sizes amongst the powder grades remained the same, which is consistent with the PSD results shown in Fig. 3. In our study, 1GNP/PVA-PA12 powder had the lower BFE and SE value. This is a result of changing particle surface by adding GNP and possibly

reducing inter-particle friction, GNP being known to improve wear properties [18, 19]. The stability index in Fig. 6 shows no significant change amongst the four powders, a sign that the powder is not affected by attrition or segregation during the test.

Table 5. BFE, SE, CBD and SI values of all powders

Material	BFE (mJ)	SE (mJ/g)	CBD (g/ml)	SI
PA12	208.18 ± 3.85	6.61 ± 0.12	0.47 ± 0.001	0.93 ± 0
PVA-PA12	155.26 ± 13.26	6.17 ± 0.23	0.47 ± 0.001	1.03 ± 0.1
0.1GNP/PVA-PA12	138.00 ± 12.36	5.20 ± 0.19	0.47 ± 0.004	0.98 ± 0
1GNP/PVA-PA12	113.70 ± 6.22	5.33 ± 0.28	0.49 ± 0.003	0.97 ± 0

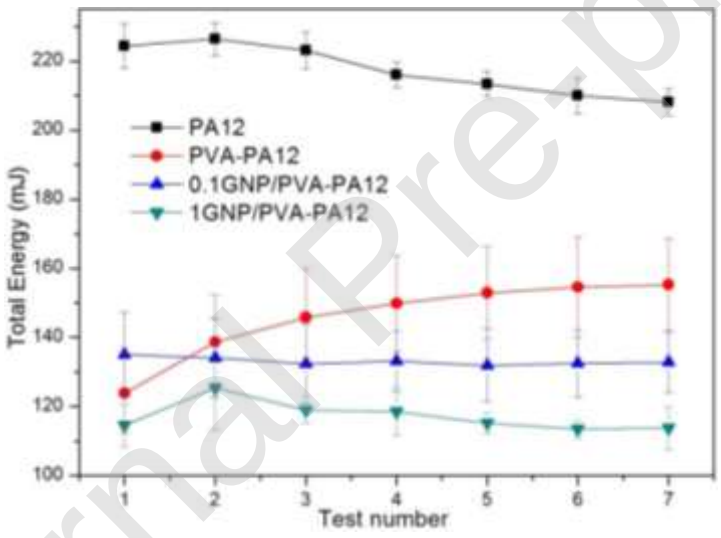

Fig. 6. Stability test of PA12 and PVA coated powders

3.4 Nanoparticle exposure in air

The release of nanoparticles in air was monitored for all powder grades as well as 1GNP-PA12 dry-mix grade. The lung deposited surface area (LDSA) was measured in in a filtered extraction cabinet at three steps (Stabilisation, Mixing and Stabilisation)

at both low and high positions (Fig. 7a and Fig. S7). Three typical measured traces of PA12, 1GNP-PA12 dry-mix and 1GNP/PVA-PA12 powders at low position are shown in Fig. 7a. The maximum LDSA values of plain PA12 and 1GNP/PVA-PA12 powders at low position are very similar, which are around 100, suggesting that the GNP have been successfully encapsulated in the PVA coating. The maximum LDSA value of 1GNP-PA12 dry-mix powder is as high as 2380, which is about 27 times higher than that of plain PA12 and 1GNP/PVA-PA12 powders. Such high LDSA value is caused by the presence of loose GNPs in air which suggests that using dry-mix powders for LS is not suitable.

The recorded data of other powders are summarised and plotted in Fig. S8-S11. The LDSA value at the high position is much lower than that of the low position. This is probably due to the air particle settling down after mixing. Fig. 7b summaries the LDSA ranges between different at low and high position. The maximum LDSA values of 0.1GNP/PVA-PA12 and 1GNP/PVA-PA12 powders are both much lower than that of dry-mix one and close to that of plain PA12 powder. Therefore, it confirms that the GNP has been successfully encapsulated inside the PVA coating, and it is safe to use the core-shelled powders for LS.

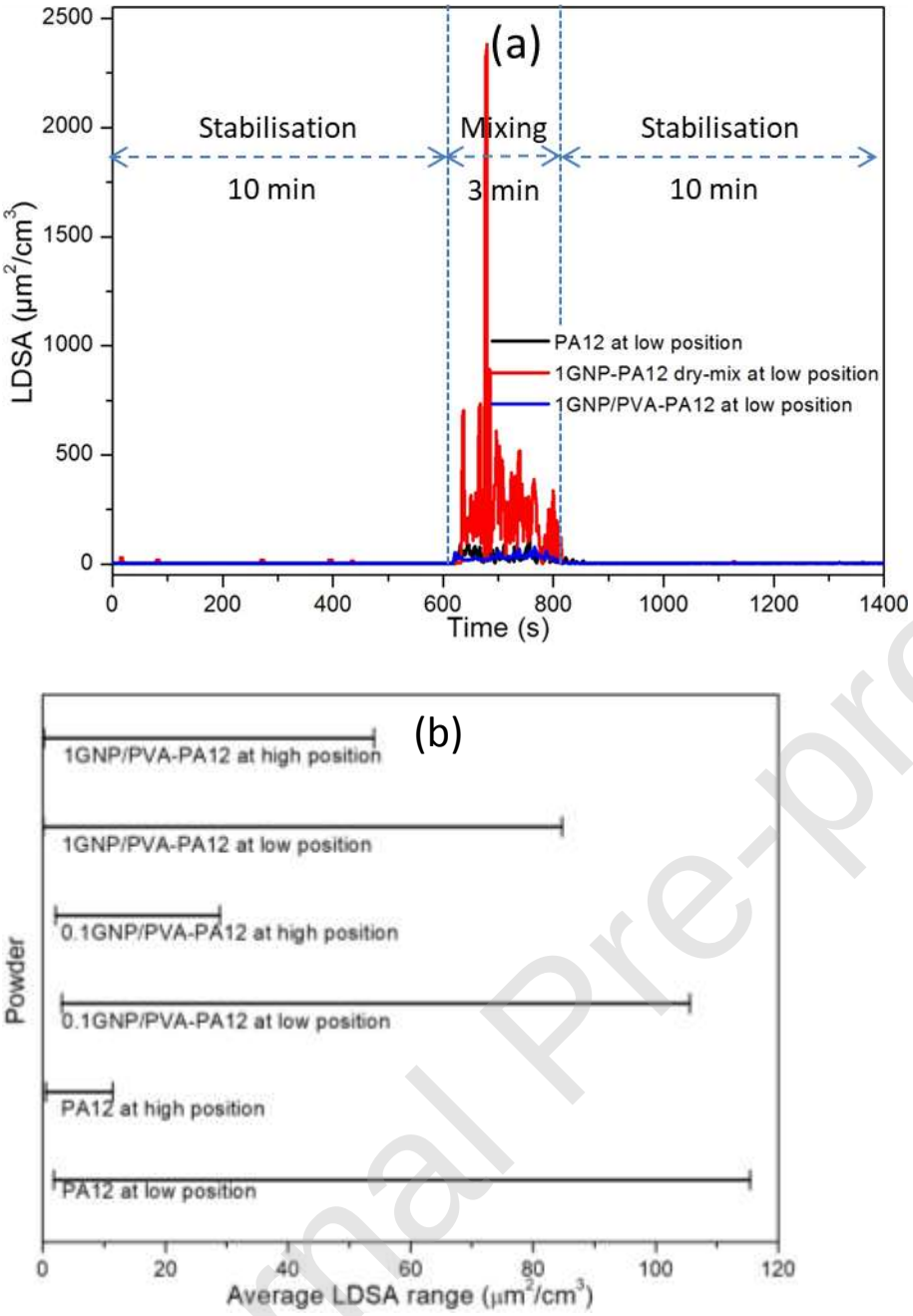

Fig. 7. (a) Air monitor recorded data in three steps (10-min Stabilisation; 3-min Mixing; and 10-min Stabilisation) for PA12, 1GNP-PA12 dry-mix and 1GNP/PVA-PA12 powders at low position; (b) Average LDSA range as a function of powders measured in low and high position

3.5 Characterisation of Laser-Sintered Parts

After successful LS (shown in Fig. S12), the mechanical properties of the LS parts were evaluated using standard tensile, compression, and 3-point bending tests. Previous studies showed that concentrations of up to 0.5 wt% tend to improve mechanical performance, where higher concentrations (higher than 1 wt%) show a significant improvement in electrically and thermally conducting properties [3]. As this study is focused on mechanical data, the core-shell powder with 0.1GNP was selected for laser sintering [8].

The mechanical results are shown in Table 6 and statistical results in Table 7. The typical stress-strain curves of laser-sintered parts are presented in Fig. 8. Tensile strengths of the three materials are significantly different ($p < 0.001$ for all three pairs), increasing from 44 MPa for PA12 to 47 MPa in the case of PVA-PA12 and 50 MPa for 0.1GNP/PVA-PA12. Previous studies of injection moulded PVA-PA6 samples (blended using a twin screw extruder) showed a sharp drop in tensile strength at yield from 46 N/mm^2 in the case of PA6 to 38 N/mm^2 when 5 wt% PVA was added [20]. The authors claimed that the drop in performance is related with variation in phase morphology and hydrophilicity but these theories are not explained further [20]. The authors also highlighted the presence of a yield stress accompanied by the formation of necking followed by a cold drawing [20]. Although the combination of materials is relevant to our study, the manufacturing methods will significantly impact on the microstructure and mechanical results, therefore the results are different. In this study, the method of incorporation of PVA into the PA12 does not involve any mechanical mixing, which normally will allow a formation of a better homogenous blend. The shear rates in laser

sintering process are negligible in comparison with any form of mechanical mixing. The elongation of break is known to be significantly lower in laser sintered samples in comparison with injection moulded samples. As it can be seen in Figure 8, no yield stress is present in any of the laser sintered samples (plain PA12 or PVA-PA12). In addition, the concentration of PVA within the PVA-PA12 blend is only 2 wt% significantly less than any other previous studies [16, 20, 21], where, in general, the PVA quantities to nylons are ranging from 5 to 75 wt% PVA.

The strain at break does not significantly vary among three materials (shown in Table 7). The mean strain at break is similar for 0.1GNP/PVA-PA12 samples and plain PA12 samples (23.5%). Whilst PVA-PA12 samples show borderline significantly lower mean strain at break comparing to the other two materials. Plain PVA is known to have a high elongation of break of 266%, but it seems that PVA is not influencing the strain of its blends, which is due to the small concentrations used [22]. Previous studies observed that the addition of nanoparticles leads to a decrease in strain at break even though other mechanical properties, such as Young's modulus, yield strength, flexural stress, or flexural modulus increase [4, 5, 23]. The decrease in strain at break was previously attributed to the poor dispersion of filler in the matrix [8, 24].

The core-shell structure significantly increases the tensile modulus. Mean tensile moduli increased from 1.50 GPa for plain PA12 samples to 1.62 GPa for 0.1GNP/PVA-PA12 samples and 1.61 GPa for PVA-PA12 ($p < 0.003$ in both cases). However, the presence of 0.1GNP within the shell does not significantly improve the tensile modulus comparing to PVA-PA12 samples ($p = 0.9408$).

For the compression test results, PVA-PA12 samples exhibit similar mean compression stress and mean modulus to those of plain PA12 ($p = 0.0534$ and $p =$

0.9183, respectively), indicating that PVA has negligible effect on the compression, the laser sintered parts are not changing their structural integrity (e.g. density and porosity) due to the addition of 2 wt% PVA. On the contrary, the presence of 0.1GNP significantly improves the compression stress ($p < 0.0001$ to plain PA12 and $p = 0.0003$ to PVA-PA12) and the compression modulus ($p = 0.0263$ to plain PA12). This could be the result of several factors: 1) the addition of graphene improves the IR thermal absorption, increases the energy absorbed during the laser sintering process, consolidating even better the parts; 2) the mechanical benefits of graphene are transferred to the PVA-PA12 structure.

In the case of the 3-point bending tests, 0.1GNP/PVA-PA12 significantly enhances the mean flexural modulus comparing to plain PA12 samples ($p = 0.0107$). However, the differences between 0.1GNP/PVA-PA12 and PVA-PA12 ($p = 0.1489$) or between PVA-PA12 and plain PA12 ($p = 0.4544$) are not significant.

Young et al. used theoretical analysis and experimental stress-induced Raman band shifts to understand the mechanics of GNP reinforcement within polymers [25]. The study was found that the orientation of the GNP and the strength of the interface between the GNP and polymer are the two keys factors for reinforcement. In our study, the orientation of GNP in the laser sintered parts is random and therefore should allow fabrication of isotropic structures, an important feature for the laser sintered part known to be highly anisotropic. The interface plays an important role to enhance the mechanical properties. In this study, the GNP have not been functionalised, the interface is not be sufficiently improved hence explaining the modest improvement in mechanical properties.

The fracture surfaces of the PVA-PA12 and 0.1GNP/PVA-PA12 LS parts were observed by SEM (shown in Fig. 10a, 10b and Fig. S13). Voids were noticed in both PVA-PA12 and 0.1GNP/PVA-PA12 parts. This could be the result of slow particle coalescence as shown by the melt flow index results, however this can be addressed by selecting a PVA grade of a lower M_W. Fig. 10c shows the fracture surface of the tensile test samples. The surface presents brittle as well as ductile regions with GNP well embedded and distributed within the matrix (shown in Fig. 10d).

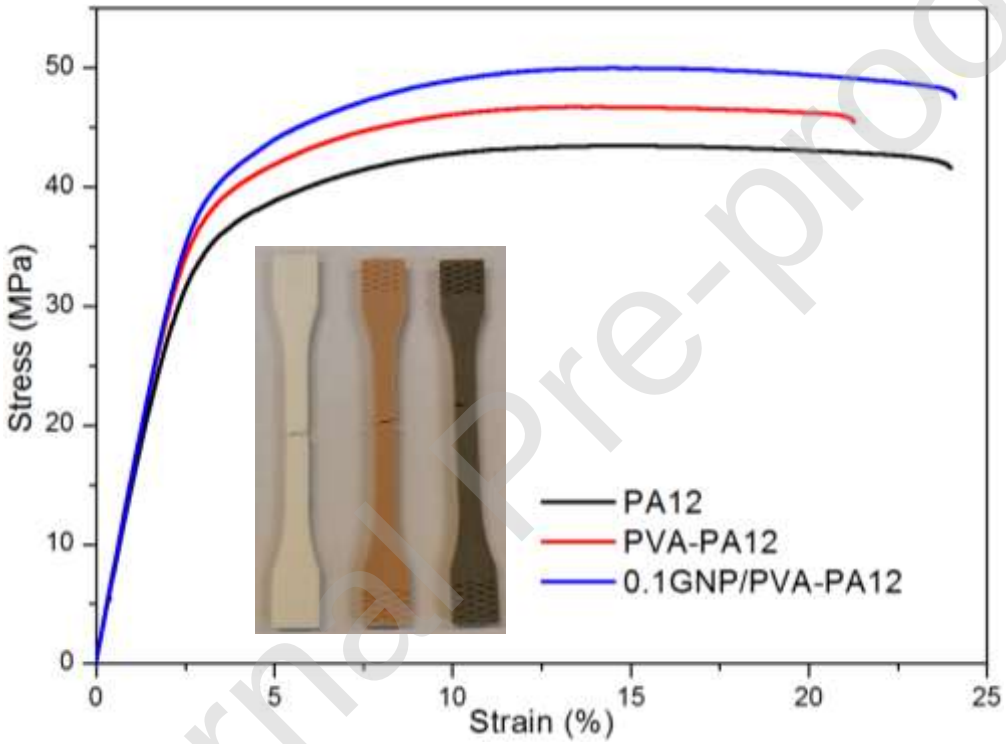

Fig. 8. Typical tensile strain-stress of the laser-sintered parts with an inset of the broken laser-sintered specimens. The PVA-PA12 samples had a yellowish, light brown colour possibly due to a slight thermo-oxidative effect.

Table 6. Mechanical properties of laser-sintered parts

		PA12	PVA-PA12	0.1GNP/PVA-PA12
Tensile Test	Tensile Strength (MPa)	44.1 ± 1.6	47.2 ± 0.6	50.1 ± 0.8

	Strain at Break (%)	23.5 ± 4.1	20.0 ± 1.8	23.5 ± 2.3
	Tensile Modulus (GPa)	1.50 ± 0.20	1.61 ± 0.10	1.62 ± 0.10
Compression Test	Compression stress (MPa)	46.3 ± 1.2	47.8 ± 1.2	50.5 ± 1.2
	Compression Modulus (GPa)	1.0 ± 0.1	1.0 ± 0.1	1.2 ± 0.1
3-point bending Test	Flexural Stress at Strain of 10% (MPa)	40.3 ± 1.6	45.3 ± 1.0	44.1 ± 2.2
	Flexural Modulus (MPa)	1354.8 ± 39.3	1420.1 ± 76.1	1523.9 ± 47.9

Table 7. Statistical results of the mechanical testing data

Groups	P-value	Conclusion
Tensile strength		
PVA-PA12 & PA12	<0.0001	Significantly different
0.1GNP/PVA-PA12 & PA12	<0.0001	Significantly different
0.1GNP/PVA-PA12 & PVA-PA12	<0.0001	Significantly different
Strain		
PVA-PA12 & PA12	0.0882	Not different
0.1GNP/PVA-PA12 & PA12	0.9994	Not different
0.1GNP/PVA-PA12 & PVA-PA12	0.1059	Not different
Tensile Modulus		
PVA-PA12 & PA12	0.0029	Significantly different
0.1GNP/PVA-PA12 & PA12	0.0021	Significantly different
0.1GNP/PVA-PA12 & PVA-PA12	0.9408	Not different
Compression strength		
PVA-PA12 & PA12	0.0534	Not different
0.1GNP/PVA-PA12 & PA12	<0.0001	Significantly different
0.1GNP/PVA-PA12 & PVA-PA12	0.0003	Significantly different
Compression Modulus		
PVA-PA12 & PA12	0.9183	Not different
0.1GNP/PVA-PA12 & PA12	0.0263	Significantly different
0.1GNP/PVA-PA12 & PVA-PA12	0.0859	Not different
Flexural Modulus		
PVA-PA12 & PA12	0.4544	Not different
0.1GNP/PVA-PA12 & PA12	0.0107	Significantly different
0.1GNP/PVA-PA12 & PVA-PA12	0.1489	Not different

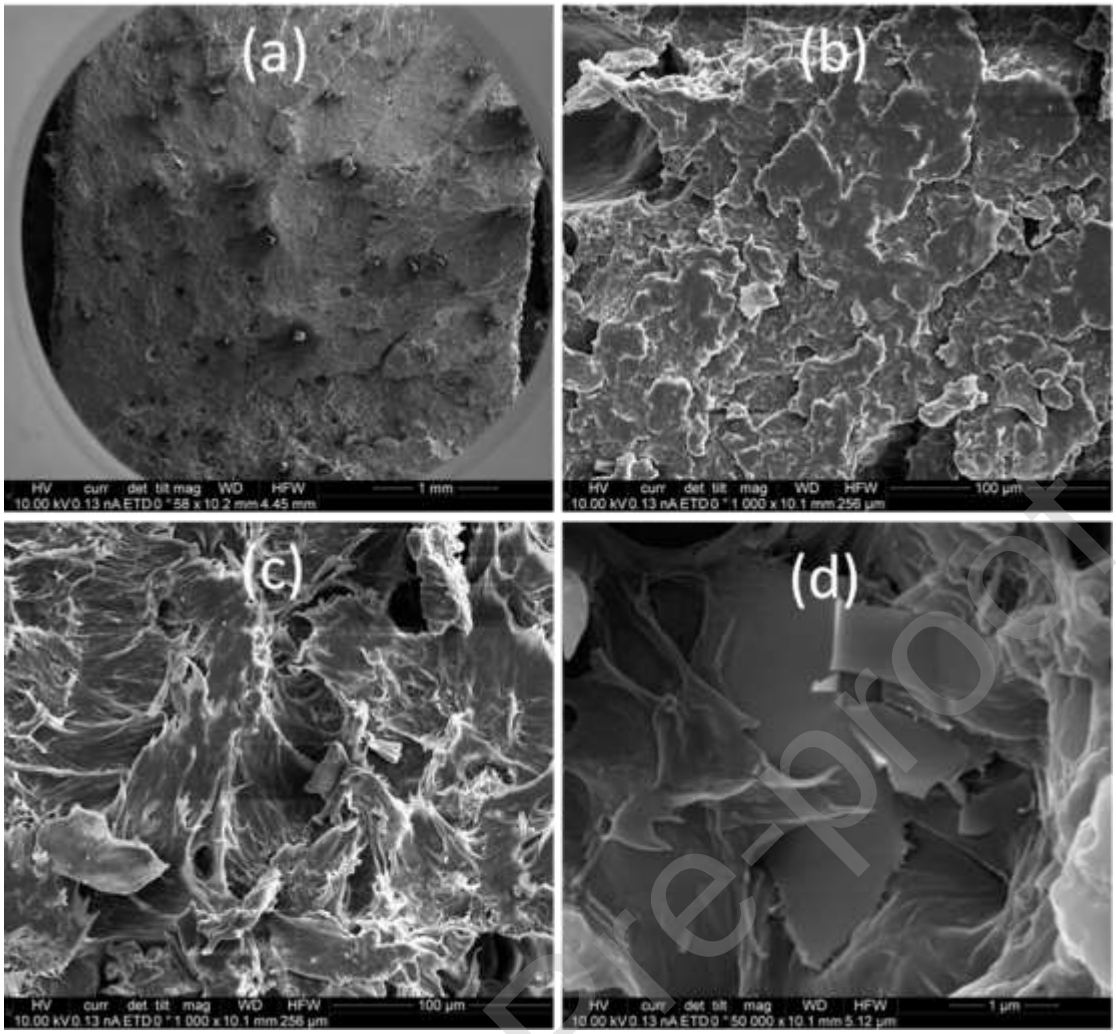

Fig. 9. SEM images of fracture surface of 0.1GNP/PVA-PA12 laser-sintered tensile bars under (a-c) low and (d) high magnification

4. Conclusions

This work presented a new method of fabrication of nanocomposite powders, scalable and environmentally safe, avoiding the use of solvents. The new nanocomposite powder had good properties: similar PSD as the plain PA12 powder, smoother surface and better flow properties. The production of PVA coated PA12 particles with GNP encapsulated into the PVA coating was confirmed by SEM and TEM. The measured LDSA values at different locations within the fume cupboard of plain

polymer, dry blend and the new core-shell powders confirmed that the GNP has been successfully encapsulated in PVA-PA12 matrix and the new powder is safe to be used. The GNP/PVA-PA12 powder has shown faster crystallisation time than those of plain PA12 and PVA-PA12 powder. The mechanical properties of 0.1GNP/PVA-PA12 LS parts exhibited a modest improvement in tensile, compression and 3-point bending test, and the break strain is comparable to the plain PA12.

Author statement

Binling Chen: Formal analysis, Investigation, Writing - Original Draft

Richard Davies: Methodology, Writing- Reviewing and Editing

Yaan Liu: Formal analysis, Writing- Reviewing and Editing

Nan Yi: Formal analysis, Writing - Review & Editing

Dayuan Qiang: Writing- Reviewing and Editing

Yanqiu Zhu: Writing - Review & Editing

Oana Ghita: Conceptualization, Supervision, Writing - Review & Editing

Declaration of competing interest

The authors declare no conflict of interest.

Declaration of interests

The authors declare that they have no known competing financial interests or personal relationships that could have appeared to influence the work reported in this paper.

Acknowledgements

The authors would like to thank the UK Engineering and Physical Science Research Council for its funding (EPSRC grant - Novel high performance polymeric composite materials for additive manufacturing of multifunctional components EP/N034627/1), and Ms Ana Correia and Dr Christian Hacker for their kind help with the TEM sample preparation.

Appendix A. Supplementary data

Supplementary data associated with this article can be found.

References

[1] EOS, https://www.eos.info/material-p, in, 2018.

[2] B. Chen, Y. Wang, S. Berretta, O. Ghita, Poly Aryl Ether Ketones (PAEKs) and carbon-reinforced PAEK powders for laser sintering, J. Mater. Sci., (2017) 1-16.

[3] B. Chen, S. Berretta, K. Evans, K. Smith, O. Ghita, A primary study into graphene/polyether ether ketone (PEEK) nanocomposite for laser sintering, Appl. Surf. Sci., 428 (2018) 1018-1028.

[4] Y. Chunze, S. Yusheng, Y. Jinsong, L. Jinhui, A Nanosilica/Nylon-12 Composite Powder for Selective Laser Sintering, J. Reinf. Plast. Compos., 28 (2009) 2889-2902.

[5] Y.S.S. C.Z. Yan, J.S. Yang and J.H. Liu, An organically modified montmorillonite/nylon‐12 composite powder for selective laser sintering, Rapid Prototyp. J., 17 (2011) 28-36.

[6] C. Yan, L. Hao, L. Xu, Y. Shi, Preparation, characterisation and processing of carbon fibre/polyamide-12 composites for selective laser sintering, Compos. Sci. Technol., 71 (2011) 1834-1841.

[7] W. Zhu, C. Yan, Y. Shi, S. Wen, J. Liu, Q. Wei, Y. Shi, A novel method based on selective laser sintering for preparing high-performance carbon fibres/polyamide12/epoxy ternary composites, Sci. Rep., 6 (2016) 33780.

[8] J. Bai, R.D. Goodridge, R.J.M. Hague, M. Song, Improving the mechanical properties of laser-sintered polyamide 12 through incorporation of carbon nanotubes, Polym. Eng. Sci,, 53 (2013) 1937-1946.

[9] J. Bai, R.D. Goodridge, R.J.M. Hague, M. Song, H. Murakami, Nanostructural characterization of carbon nanotubes in laser-sintered polyamide 12 by 3D-TEM, J. Mater. Res., 29 (2014) 1817-1823.

[10] J. Bai, R.D. Goodridge, R.J.M. Hague, M. Song, M. Okamoto, Influence of carbon nanotubes on the rheology and dynamic mechanical properties of polyamide-12 for laser sintering, Polym. Test., 36 (2014) 95-100.

[11] J. Bai, R. Goodridge, S. Yuan, K. Zhou, C. Chua, J. Wei, Thermal Influence of CNT on the Polyamide 12 Nanocomposite for Selective Laser Sintering, Molecules, 20 (2015) 19041.

[12] A.C. de Leon, B.J. Rodier, C. Bajamundi, A. Espera, P. Wei, J.G. Kwon, J. Williams, F. Ilijasic, R.C. Advincula, E. Pentzer, Plastic Metal-Free Electric Motor by 3D Printing of Graphene-Polyamide Powder, ACS Appl. Energy Mater., 1 (2018) 1726-1733.

[13] T. Hupfeld, T. Laumer, T. Stichel, T. Schuffenhauer, J. Heberle, M. Schmidt, S. Barcikowski, B. Gökce, A new approach to coat PA12 powders with laser-generated nanoparticles for selective laser sintering, Procedia CIRP, 74 (2018) 244-248.

[14] B. Chen, B. Yazdani, L. Benedetti, H. Chang, Y. Zhu, O. Ghita, Fabrication of nanocomposite powders with a core-shell structure, Compos. Sci. Technol., 170 (2019) 116-127.

[15] S. Berretta, K.E. Evans, O.R. Ghita, Predicting processing parameters in high temperature laser sintering (HT-LS) from powder properties, Mater. Des., 105 (2016) 301-314.

[16] E.G. Koulouri, J.K. Kallitsis, Miscibility behavior of Poly(vinyl alcohol)/Nylon 6 blends and their reactive blending with Poly(ethylene-co-ethyl acrylate), Polymer, 39 (1998) 2373-2379.

[17] L. Altay, M. Atagur, K. Sever, I. Sen, T. Uysalman, Y. Seki, M. Sarikanat, Synergistic effects of graphene nanoplatelets in thermally conductive synthetic graphite filled polypropylene composite, Polym. Compos., 40 (2019) 277-287.

[18] D. Berman, A. Erdemir, A.V. Sumant, Graphene: a new emerging lubricant, Mater. Today, 17 (2014) 31-42.

[19] B. Gullac, O. Akalin, Frictional Characteristics of IF-WS2 Nanoparticles in Simulated Engine Conditions, Tribol. Trans., 53 (2010) 939-947.

[20] B. Ramaraj, P. Poomalai, Development of potentially biodegradable polyamide‐6 and polyvinyl alcohol blends: Physico‐mechanical properties, thermal properties, and soil test. J. Appl. Polym. Sci., 98 (2005) 2339-2346.

[21] Y. Huang, D. Dai, H. Li, L. Sun, J. Runt, K. Huang, J. Yeh, Oxygen barrier, free volume, and blending properties of fully bio‐based polyamide 11/poly(vinyl alcohol) blends. J Appl Polym Sci, 137 (2020), 48562-48570.

[22] I. Korbag, S.M. Saleh (2016) Studies on mechanical and biodegradability properties of PVA/lignin blend films, Int. J. Environ. Stud., 73 (2016), 18-24.

[23] G.V. Salmoria, R.A. Paggi, A. Lago, V.E. Beal, Microstructural and mechanical characterization of PA12/MWCNTs nanocomposite manufactured by selective laser sintering, Polym. Test., 30 (2011) 611-615.

[24] P.K. Jain, P.M. Pandey, P.V.M. Rao, Selective laser sintering of clay-reinforced polyamide, Polym. Compos., 31 (2010) 732-743.

[25] R. J. Young, M. Liu, I. A. Kinloch, S. Li, X. Zhao, C. Vallés, D. G. Papageorgiou, The mechanics of reinforcement of polymers by graphene nanoplatelets, Compos. Sci. Technol., 154 (2018), 110-116.